
MIXRTs: Toward Interpretable Multi-Agent Reinforcement Learning via Mixing Recurrent Soft Decision Trees

Zichuan Liu, Yuanyang Zhu, Zhi Wang, Yang Gao, Chunlin Chen

Nanjing University, Nanjing 210093, China

lzc775269512@gmail.com, yuanyang@smail.nju.edu.cn
 zhiwang@nju.edu.cn, gaoy@nju.edu.cn, clchen@nju.edu.cn

Abstract

Multi-agent reinforcement learning (MARL) recently has achieved tremendous success in a wide range of fields. However, with a black-box neural network architecture, existing MARL methods make decisions in an opaque fashion that hinders humans from understanding the learned knowledge and how input observations influence decisions. Our solution is MIXing Recurrent soft decision Trees (MIXRTs), a novel interpretable architecture that can represent explicit decision processes via the root-to-leaf path of decision trees. We introduce a novel recurrent structure in soft decision trees to address partial observability, and estimate joint action values via linearly mixing outputs of recurrent trees based on local observations only. Theoretical analysis shows that MIXRTs guarantees the structural constraint with additivity and monotonicity in factorization. We evaluate MIXRTs on a range of challenging StarCraft II tasks. Experimental results show that our interpretable learning framework obtains competitive performance compared to widely investigated baselines, and delivers more straightforward explanations and domain knowledge of the decision processes.

1 Introduction

Multi-agent reinforcement learning (MARL) has proven to be a considerable promise for addressing a variety of challenging tasks [1, 2]. Despite their promising performance, the advancements are mainly attributed to utilizing deep neural networks (DNNs) models as stronger function approximators, which are encoded with thousands to millions of parameters interacting in complex and non-linear ways. This sort of architecture brings excellent hindrances for humans or experts to understand how decisions are taken and what key feature information influences decisions, especially as networks grow deeper in size or add more complex architecture. Indeed, creating mechanisms to interpret the implicit behaviors of DNNs themselves remains an open problem in the field of machine learning [3, 4].

In high-stakes domains, such as healthcare, aviation and policy making, it is crucial to gain insight into the decision-making process of the machine. It imposes significant limitations on practitioners applying MARL techniques, as the lack of transparency creates critical barriers to establishing trust in the policies of agents and scrutinizing policy weaknesses [5]. The explainable reinforcement learning (XRL) is a promising approach to generating procedures that can be followed step-by-step or held accountable by human operators. While existing XRL methods offer much promise [6, 7] in single-agent tasks, they still can not match the performance of the look-ahead deep RL techniques [8].

Differentiable soft decision trees (SDTs) [9, 10], based on the structure of fuzzy decision trees whose model expressivity lies in the middle of traditional DTs and neural networks [11], are usually regarded as models with readable interpretations for humans, which can be easily visualized and simulated

even by non-experts. Existing works [12, 13] have utilized differentiable SDTs for interpreting RL, mainly consisting of an imitation learning method and a full RL learning. With the imitating learning paradigm, the imitators learn the implicit knowledge from RL agents with black-box models, which can generate human-understandable decision rules. However, the performance of the opaque DRL models constrains the mimic performance of the tree, which also brings challenges to optimizing the fidelity jointly with the simplicity of tree models to find a “sweet spot”.

An alternative approach is full RL learning, which directly learns the dominant knowledge from the tasks with interpretable models. While SDTs have achieved a better balance between interpretability and performance in single-agent and simple tasks (e.g., CartPole and MountainCar in OpenAI Gym [14]) [13], they could not maintain well performance without sacrificing interpretability in complex tasks since limited model expressivity. Particularly, to our knowledge in the RL community, there have been no existing works exploring the interpretability of the models in the MARL problems. Here, we aim at a more efficient and explicit interpretable architecture that looks ahead to achieving promising performance with tree-based explainable models in multi-agent challenging tasks.

In this paper, we propose a novel MIXing Recurrent soft decision Trees (MIXRTs) method to address the tension between performance and interpretability in the multi-agent domains. Instead of trying to understand how a deep neural network makes its decisions, we directly design recurrent tree cells (RTCs) to factorize the joint action-value function into a much richer individual class of action-value functions, where the decision process is easy to explain and engage with. To facilitate learning over longer timescales, we utilize recurrent soft decision trees that receive the current individual observation and history information as input at each timestamp. Further, we employ the ensemble mechanism that uses a linear combination of RTCs to improve performance and reduce the variance of a single decision tree. MIXRTs consists of a shared-weighted individual RTCs representing the individual value function, and mixing trees that combine them into a fully centralized state-action value function in a linear way that ensures consistency between the centralized and decentralized policies. We evaluate MIXRTs on a range of maps in StarCraft II [15]. Empirical results on more challenging tasks demonstrate that our concise learning architecture delivers simpler explanations with competitive performance. Specifically, MIXRTs finds more desirable optimal policies in easy scenarios compared to the baselines like the widely investigated QMIX [16] and QTRAN [17].

2 Background

Dec-POMDP The fully cooperative multi-agent tasks are generally modeled as Dec-POMDP [18] that consist of a tuple $\langle \mathcal{S}, \mathcal{U}, \mathcal{P}, r, \mathcal{Z}, \mathcal{O}, n, \gamma \rangle$, where $s \in \mathcal{S}$ describes the global state. At each time step, each agent $i \in \{1, \dots, n\}$ receives an observation $o_i \in \mathcal{O}_i$ from the partial observation $Z(S, i)$, and chooses an action $u_i \in \mathcal{U}$, giving rise to a joint action $\mathbf{u} := [u_i]_{i=1}^n \in \mathcal{U}^n$. This results in a transition to next state $s' \sim P(s' | s, \mathbf{u})$, and a joint reward signal $r(s, \mathbf{u})$. For each agent i , the action-observation history is $\tau_i \in \mathcal{T} := (\mathcal{Z} \times \mathcal{U})^*$, where it can condition its stochastic policy $\pi^i(u^i | \tau^i) : \mathcal{T} \times \mathcal{U} \rightarrow [0, 1]$. The goal is to find an optimal joint policy $\pi = \langle \pi_1, \dots, \pi_n \rangle$ to maximize the joint value function $Q^\pi(s_t, \mathbf{u}_t) = \mathbb{E} [\sum_{i=0}^{\infty} \gamma^i r_{t+i}]$.

Multi-agent Q-learning. Multi-agent Q-learning is a popular value-based [19, 17, 20] approach extending from deep Q-learning [21, 22]. Given transition tuples (s, \mathbf{u}, r, s') from the replay buffer stores \mathcal{B} , Θ is learnt by minimizing the squared loss $\mathcal{L}(\Theta)$ on the temporal-difference (TD) error $\sigma = y' - Q_{tot}(s, \mathbf{u}; \Theta)$, where $y' = r + \gamma \max_{\mathbf{u}'} Q_{tot}(s', \mathbf{u}'; \Theta')$ is the target. The parameters Θ' from a target network are periodically copied from Θ and remain constant over multiple iterations.

Centralized training and decentralized execution (CTDE). CTDE [23, 24] is an advanced paradigm for cooperative multi-agent reinforcement learning. In CTDE fashion, action-observation values of all agents and global states are collected through a central controller during training. However, in the execution phase, each agent has its own policy network to make decisions based on its individual action-observation history. The individual-global-max (IGM) property [17] is a popular principle to realize effective CTDE as

$$\arg \max_{\mathbf{u}} Q_{tot}(\tau, \mathbf{u}) = \left(\arg \max_{u_1} Q_1(\tau_1, u_1), \dots, \arg \max_{u_n} Q_n(\tau_n, u_n) \right), \quad (1)$$

where τ represents the history record of joint action-observation and Q_{tot} represents the joint Q -function for each individual action-value function $Q_i(\tau_i, u_i)$. Both VDN [19] and QMIX [16] are

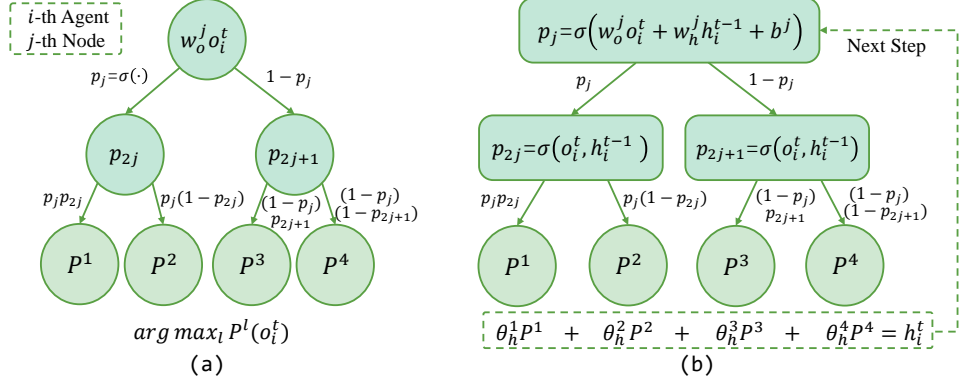


Figure 1: Soft decision tree and the process of a recurrent tree cell. (a) is a two-level soft decision tree. (b) illustrates the process of a two-level recurrent tree cell that receives the current individual observation o_i^t and the historical leaf information h_i^{t-1} as input at each timestamp.

popular CTDE methods for estimating the optimal Q_{tot} via the combined agents of Q_i . In VDN, the Q_{tot} is calculated by summing the utilities of each agent as $Q_{tot}(\tau, \mathbf{u}) = \sum_{i=1}^n Q_i(\tau_i, u_i)$. And QMIX combines Q_i through the state-dependent non-linear monotonic function f_s : $Q_{tot}(\tau, \mathbf{u}) = f_s(Q_1(\tau_1, u_1), \dots, Q_i(\tau_i, u_i), \dots, Q_n(\tau_n, u_n))$, where $\frac{\partial f_s}{\partial Q_i} \geq 0, \forall i \in \{1, \dots, n\}$.

Soft decision trees (SDTs). Differentiable decision tree [25, 26] has shown to be more accurate than traditional hard decision trees. Especially, SDT [9] with binary probabilistic decision bounds has favorable transparency and performance in reinforcement learning tasks [12, 13]. On a given observation o^t , each inner node j calculates the probability for traversing to the left child node as

$$p_j(o^t) = \sigma(w_o^j o^t + b^j), \quad (2)$$

where σ is the sigmoid function, and w^j, b^j are a weight vector parameter and a bias parameter, respectively. The learned model consists of a hierarchy of filters that assign the input observation to a particular leaf node with a particular path probability $P^l(o^t)$, producing a probability distribution over the action class. We select action with the largest probability $l^* = \arg \max_l P^l(o^t)$, and the output value of the maximum probability is $Q^{l^*} = \text{softmax}(\theta^{l^*})$, where $\theta \in \mathbb{R}^U$ is a learnable parameter at the l -th leaf.

3 Recurrent Tree Cells

In this section, we propose recurrent tree cells (RTCs) that introduce recurrency into a soft decision tree to acquire the previous information, and enhance the fidelity of the Q -value by ensemble technique. First, we propose an RTC method that receives the current individual observation and relies on historical information to capture long-term dependencies in partial observation tasks. Then, we utilize a linear combination of RTCs via an ensemble mechanism to yield high performance and reduce the variance of the model while retaining simplicity.

Recurrent Tree Cell. As shown in Fig. 1(a), the SDT is a simple and univariate differentiable DT with a probabilistic decision boundary at each filter. However, SDT weakly captures a useful summary statistic for sequential decision tasks over longer timescales. Indeed by adding recurrency to a deep Q -network with a recurrent neural network instead of the fully-connected layer [27] in partially-observable tasks, agents can effectively capture long-term dependencies conditioning on their entire action-observation history. Inspired by recurrent architecture, we propose a recurrent tree cell (RTC) for tracking information that receives the current individual observation o_i^t and history embedding h_i^{t-1} as input at each time step, where we extract the information of the previous hidden state for each agent i , as shown in Fig. 1(b).

Combining the recurrent architecture, for each non-leaf node, RTC learns linear filters in its branching node to traverse to the left child node with the probability

$$p_j(o_i^t, h_i^{t-1}) = \sigma(w_o^j o_i^t + w_h^j h_i^{t-1} + b^j), \quad (3)$$

where b^j is a bias learnable parameter, and w_o^j, w_h^j are the learnable parameters for the feature vector of the observation o_i^t and the previous hidden state h_i^{t-1} , respectively. Similarly, we can obtain the probability of the right branch as $1 - p_j(o_i^t, h_i^{t-1})$, which is the same as in SDTs. Then, for each leaf node, the probability of selecting the leaf node P^l is equal to the product of the overall path probability starting from the root to the leaf node l as

$$P^l(o_i^t, h_i^{t-1}) = \prod_{j \in \text{route}(l)} p_{\lfloor j/2 \rfloor \rightarrow j}(o_i^t, h_i^{t-1})^{[l \swarrow j]} (1 - p_{\lfloor j/2 \rfloor \rightarrow j}(o_i^t, h_i^{t-1}))^{1-[l \swarrow j]}, \quad (4)$$

where $[l \swarrow j]$ denotes the boolean event $\in \{0, 1\}$, which means whether j passes the left-subtree to reach the leaf node l . With the target distribution of the tree, we measure the current hidden state h_i^t of the leaf by combining the probability values of each leaf with weight scalar θ_h^l , and provide a vector w_q that serves this tree to capture action-observation value

$$h_i^t = \sum_{l \in \text{LeafNodes}} P^l(o_i^t, h_i^{t-1}) \theta_h^l, \quad (5)$$

$$Q_i(\tau_i, \cdot) = h_i^t w_q, \quad (6)$$

where P^l is the overall path probability along the root to the leaf l , the learnable parameter θ_h^l calculates the hidden state h_i^t by multiplication with P^l , and w_q is a training parameter to transform hidden information h_i^t into action distribution. Finally, for each agent i , we choose a decentralized execution solely action u_i^t by ε -greedy methods with respect to its $Q_i(\tau_i, u_i)$.

The Ensemble of Recurrent Tree Cells. The soft decision tree exhibits several appealing properties with the multivariate tree structure, such as ease of tuning, robustness to outliers, and interpretability [13]. Considering multivariate and using all input features for each node, a single soft decision tree could lack expressiveness and have high variance on small data sets. An ensemble paradigm of decision trees, rather than a single one, is also known to reduce the variance component of the error [28, 29]. To relieve the above tension, we utilize the variance optimized bagging (Vogging) that is based on the bagging technique [30] to linearly combines the recurrent tree cells.

Hence, the individual value function for the agent i can be represented as

$$Q_i(\tau_i, \cdot) = h_{i,(1)}^t w_{q,(1)} + h_{i,(2)}^t w_{q,(2)} + \dots + h_{i,(H)}^t w_{q,(H)}, \quad (7)$$

where H be the size of ensemble RTCs, $w_{q,(1)}, w_{q,(2)}, \dots, w_{q,(H)}$ are learnable parameters to optimize a linear combination of the H trees for improving the expressiveness and reducing the variance of RTCs, and the hidden state h_i^t is derived as the vector $[h_{i,(1)}^t, h_{i,(2)}^t, \dots, h_{i,(H)}^t]$ to the express history record. With the ensemble paradigm, the RTCs produce a local policy distribution as a Q -function for each agent, and execute action via sampling with the distribution.

To maintain interpretability and simplicity, all the above functions are linear. In addition, considering shallow trees can be easily described and even be implemented by hand, it is acceptable that linearly combining the trees of depth 2 or 3 achieves impressive performance and improves the stability of the model via only sacrificing a little interpretability. In practice, a moderate value of H (e.g., $16 \sim 64$) is sufficient to obtain efficient performance, and additional ablation results are provided in Appendix F.

4 The Mixing Recurrent Soft Decision Trees Architecture

In this section, we propose a novel method called *MIXing Recurrent soft decision Trees* (MIXRTs), like QMIX, which can represent a much richer class of action-value functions. The overall architecture of MIXRTs is illustrated in Fig. 2, which consists of two main components as follows: (i) an individual action-value function for each agent, and (ii) a mixing trees component similar to the RTCs hyper-tree in which a joint action-value function Q_{tot} is factorized into individual action-value function Q_i of each agent i under the advantage-based IGM constraint. The two components are trained in a centralized manner, and each agent uses its own factorized individual action-value function Q_i to take action during decentralized execution. Each component is elaborated on next.

Individual RTCs for Action-value. The individual value function generally could be represented by an independent RTCs component for each agent. However, a large number of learnable parameters may bring confusion in understanding the decision process of the model. Inspired by [19], we utilize

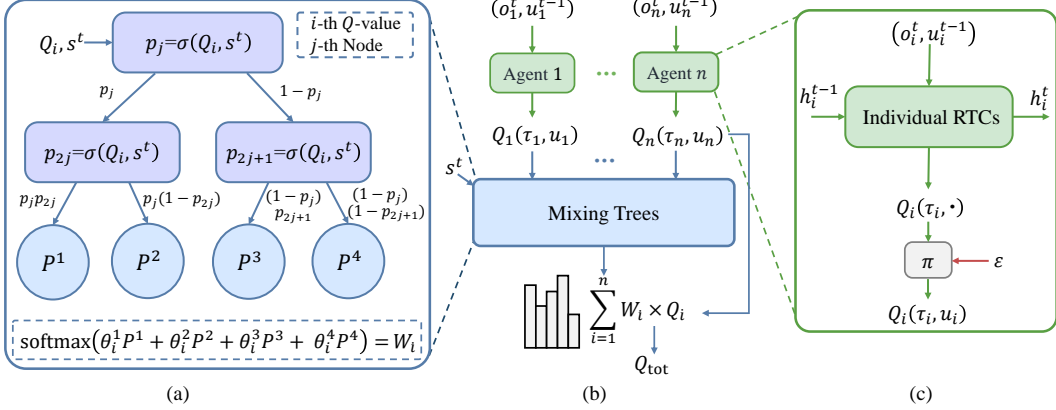


Figure 2: (a) A diagram of the mixing trees structure with depth 2. (b) The overall MIXRTs architecture. We finally obtain the joint Q_{tot} value via a linear combination of the individual action-value functions. (c) An individual RTCs structure for each agent.

hyper RTCs to share certain tree weights between agents, which can also give rise to the concept of agent invariance, and be helpful in avoiding the lazy agent problem. To keep the agent invariant, we provide the role information to the agent by a one-hot encoding of their role information, in which the role information will concatenate with each observation at the root layer. The architecture, with shared weights and information channels between agent networks, satisfies agent invariance with identical policy and improves the simplicity and interpretability with fewer parameters. For each agent i , the individual value is represented by a hyper RTCs, which takes current local observation o_i^t , previous hidden state h_i^{t-1} and previous action u_i^{t-1} as inputs and outputs local $Q_i(\tau_i, u_i)$.

Mixing Trees. The mixing trees architecture is a feed-forward ensemble tree connecting local and joint action-value functions, similar to hyper RTCs without history embedding. It incorporates the information of global state s_t into individual action-value functions during the centralized training process, and produces the weights of the local action-value in the joint action-value Q_{tot} . Unlike VDN or QMIX, we assume that the joint action-value function can be weighted by the Q -values as

$$Q_{tot}(\tau, u) \approx \sum_{i=1}^n W_i Q_i(\tau_i, u_i), \quad (8)$$

where τ and u are joint action-observation and joint action, respectively. It is still sufficient to enforce the monotonicity by imposing a constraint on the relationship between Q_{tot} and each agent Q_i , the theoretical proof of the assumption can be found in Appendix A.

In detail, we employ the interpretable hyper RTCs to obtain the weights W_i for each agent i . Each root of hyper RTCs takes individual action-value Q_i and the global state s^t vector as input as

$$p_j(Q_i, s^t) = \sigma(w_q^j Q_i + w_s^j s^t + b^j), \quad (9)$$

where w_q^j , w_s^j , and b^j are learnable parameters for each layer of the RTC. After the inference process, we can obtain the joint probability distributions P^l at the leaf node layer. Here, we utilize the same operation as the individual action-value RTCs with H trees to obtain the stable weights

$$\phi_i = \sum_{l \in \text{Leaf Nodes}} P^l(Q_i, s^t) \theta_i^l, \quad (10)$$

$$W_i = \frac{\exp(\sum_{k=1}^H \phi_{i,(k)} w_{\phi,(k)})}{\sum_{i=1}^n \exp(\sum_{k=1}^H \phi_{i,(k)} w_{\phi,(k)})}, \quad (11)$$

where θ_i^l , w_{ϕ} are the learnable parameters and the mixing weight W_i is non-negative with softmax operation to enforce the monotonicity between Q_{tot} and each Q_i .

All parameters Θ in MIXRTs are learned by sampling a number of transitions $b \in \mathcal{B}$ and minimizing the following expected squared TD-error loss as

$$\mathcal{L}(\Theta) = \mathbb{E}_{(\tau, u, r, \tau') \in b} [(y_{tot} - Q_{tot}(\tau, u; \Theta))^2], \quad (12)$$

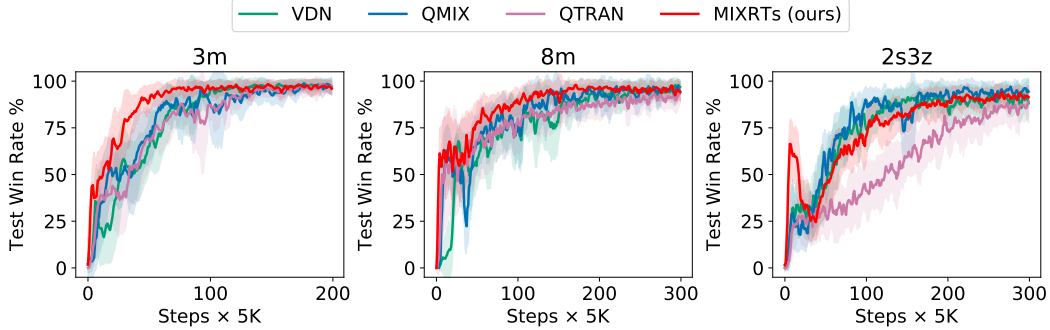


Figure 3: Median test win rates % on three easy scenarios.

and the TD target is obtained via $y_{tot} = r + \gamma \max_{\mathbf{u}'} Q_{tot}(s', \mathbf{u}'; \Theta')$. Since Eq. 1 holds, we maximize Q_{tot} in a linear fashion to achieve competitive performance, rather than scaling the exponential case.

5 Experiments

In this section, we evaluate MIXRTs on a range of StarCraft II benchmark tasks and use the representative StarCraft Multi-Agent Challenge (SMAC) scenarios as our testbed [15]. The goal of our experiments is to evaluate the performance and demonstrate the interpretability of MIXRTs. First, we compare our method with the widely investigated algorithms (VDN [19], QMIX [16] and QTRAN [17]), evaluated in easy, hard, and super hard scenarios of StarCraft II. We consider them as a comparison with special attention since they are advanced value-based methods that train decentralized policies in a centralized fashion. Additionally, we compare with the existing interpretable models SDTs [9] and CDTs [13] that decomposes into a set of simultaneous single-agent problems [31, 32], called I-SDTs and I-CDTs respectively. Further, we measure the interpretability of MIXRTs with regard to the learned tree model, aiming to present an easy-to-understand decision making process from the captured knowledge of the tasks. Finally, we perform ablation experiments to validate the effect of two key elements, both the tree depth and the number of trees. More details of the experiments and parameter settings are given in Appendix B.

5.1 Performance Comparison

Performance comparison with VDN, QMIX and QTRAN. First, we validate MIXRTs on a range of easy scenarios. As shown in Fig. 3, compared to VDN, QMIX and QTRAN methods, MIXRTs achieves competitive performance with a faster learning process. In homogeneous scenarios (e.g., 3m and 8m), MIXRTs can achieve a slightly high win rate when the number of learning steps is up to $500K$. VDN, QMIX and QTRAN obtain a sub-optimal policy whose win rates are slightly lower than those in MIXRTs. Compared to VDN and QMIX, QTRAN performs not well since the relaxations in practice could impede its precise updating [33]. Especially in the heterogeneous 2s3z map, the MIXRTs still obtain a competitive performance whose win percentage is near to QMIX, but slightly higher than VDN and QTRAN, which may benefit from the linear weights combination of the agents for efficiently performing value decomposition via ensemble paradigm.

Next, we tested the performance of different algorithms on hard and super hard scenarios. As presented in Fig. 4, MIXRTs achieves almost competitive performance in different challenging scenarios. Compared to VDN and QTRAN, MIXRTs obtains slightly better performance on a range of different challenging tasks with more efficient factorization in joint action value. Particularly on the 3s5z, MIXRTs obtains an improved performance than QMIX, which validates the effectiveness of estimating the joint action values with a linear combination of individual agent values. Except for a few challenging tasks, MIXRTs performs not well, the reason may be that MIXRTs capture weakly knowledge with a linear lightweight structure on the asymmetric scenarios. To summarize, MIXRTs achieves competitive performance and stable learning behavior while retaining the concise learning architecture with more interpretability, and more results can be referred to Fig. 8 in Appendix C.

In addition, we also analyze the simplicity of MIXRTs in terms of the number of parameters in the above baseline, which depends mainly on the observation size and the number of agents for different

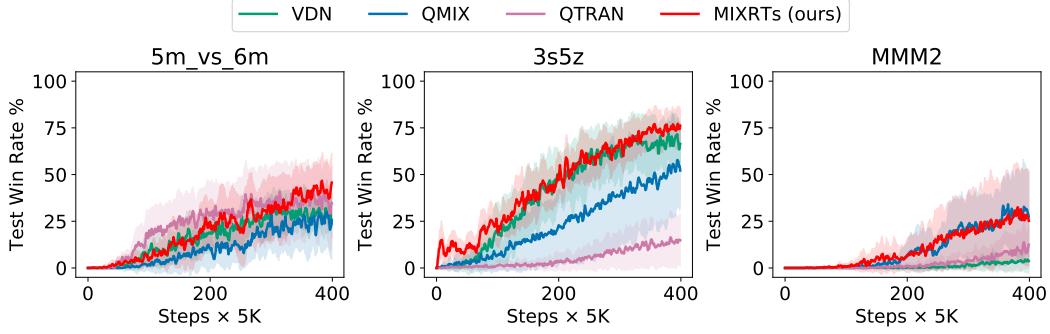


Figure 4: Median test win rates % on the hard and super hard scenarios.

Table 1: The number of parameters needs to be learned for different algorithms on different scenarios.

Method	3m	2s3z	5m_vs_6m	3s5z	8m_vs_9m	MMM2	6h_vs_8z
VDN	28,297	31,883	30,412	35,534	32,911	39,250	32,206
QMIX	37,738	62,892	55,789	111,951	96,304	173,651	72,847
QTRAN	70,911	84,437	80,518	101,492	94,513	120,320	88,436
MIXRTs (ours)	20,880	34,448	28,752	48,560	38,592	62,736	35,440

scenarios. As shown in Table 1, compared to QMIX, QTRAN and MIXRTs, the parameters that need to be learned for VDN are fewer, since there is no mixing network to represent the state-value function. Since each layer is the hierarchical structure of MIXRTs represented linearly, the number of parameters grows linearly with the depth of the tree. When the depth of the RTCs is set to 3, compared to QMIX and QTRAN, the number of parameters of MIXRTs is reduced by more than 44%, whereas it retains competitive performance. With the simplicity of the model, we can easily understand the critical features and the decision process, which strikes a better balance between performance and interpretability.

Performance comparison with I-SDTs and I-CDTs. We evaluate the learning performance of RTCs over the individual SDTs and CDTs methods on both easy and hard scenarios. As shown in Fig. 5, I-SDTs and I-CDTs do not perform well with instability on a range of tasks. One of the reasons is that the simple univariate linear structures of each filter may be difficult to represent and capture feature information in complex tasks, especially in non-stationary multi-agent tasks. In contrast, I-RTCs obtains better performance with more stability by combining high-dimensional features mapped from observations via ensemble multiple trees with historical action-observation values as input. MIXRTs outperform I-SDTs, I-CDTs and I-RTCs as assigned the joint action-observation value function of pre-agent based on RTCs to learn the linear cooperative relationship among agents, which makes an effective performance improvement compared to the existing interpretable trees.

Ablation Study. In addition, we analyze how sensitive MIXRTs is to the effect of tree depth and the number of ensemble trees on performance. We also analyze the stability of the I-SDTs, I-CDTs,

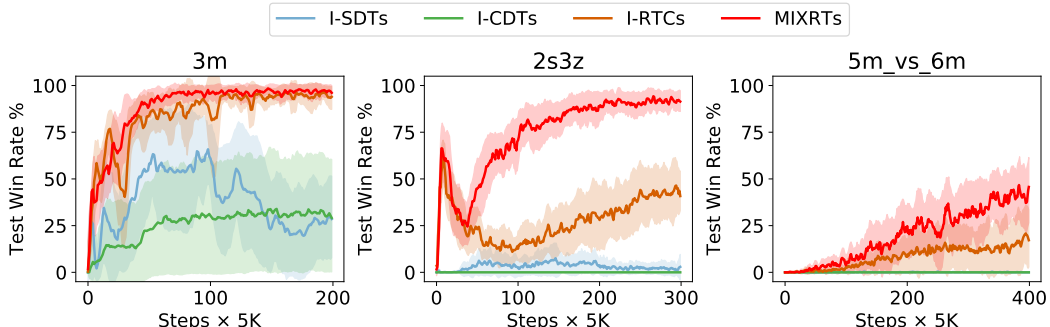


Figure 5: Median test win rates % of interpretable models on different scenarios.

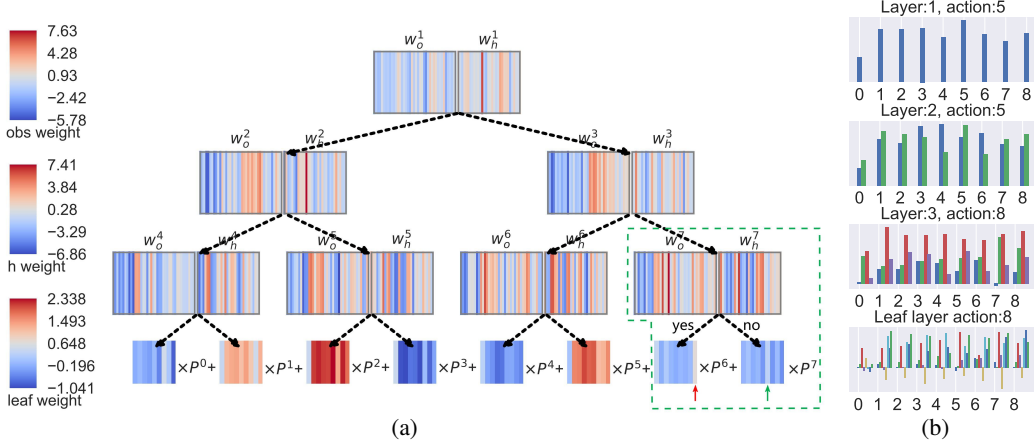


Figure 6: Heatmap visualization of the learned filters and action distributions for each layer. (a) is the heatmap visualization of the learned filters in the learned RTCs of depth 3. The weights of each non-leaf node features contain the current observations (left) and the historical records (right), respectively. The leaf nodes indicate the magnitude of the different action distributions. (b) represents the actions probability distribution of the nodes of the RTCs with given a specific observation and distinguishes each node with a different color bar.

I-RTCs and MIXRTs when the depth of the tree increases (see Appendix F for details). We suggest an appropriate value for both of the above to maintain interpretability and improve performance.

5.2 Interpretability

The main motivation for this work is to create a model whose behavior is easy to understand, mainly by fully understanding the decision process along the root-to-leaf path. To display the interpretability afforded by our approach, we describe the structure of RTCs via the learned filters at the inner nodes, and present the visualization of the learned probability action distribution. Besides, we present the importance of input features and how they influence decisions via a local explanation.

Explaining Tree Structures. The essence of RTCs is that a kind of model relies on hierarchical decisions instead of hierarchical features. The neural network generally allows the hierarchical features to learn robust and novel representations of the input space, but it will become difficult to engage with once past one or two levels. Compared to the neural network technique, we can immediately engage with each decision made at a higher level of abstraction, where each branching node of the RTCs directly processes the entire input features. By filtering different weights for each feature at each level of branching nodes of the tree, we can understand which features RTCs considers to assign a particular action distribution to a particular state and how they influence actions selected via simply examining all the learned filters along the traversed path between the root and the leaf.

As shown in Fig. 6(a), we display the structure of the learned RTCs model with a depth 3 for each agent on a 3m map, where the arrows and lines indicate the connections among tree nodes. Each node assigns different weights to each feature by processing the observed state, where a feature with a more intense color (positive: red, negative: blue) means obtaining a higher magnitude of the weight and receiving more focus. Taking the node in the green dotted area as an example, the three features with more intense color are at position 17, 14 and 29, representing the relationship with the enemy ($id = 2$), whether this enemy is visible or not, and its own health value, respectively. As these positive observations with high weights tend to move to the left leaf, it is essential to select to attack this enemy in the action distribution (marked with a red arrow). Otherwise, the leaf distributions assign probabilities to actions related to moving westward (marked with a green arrow). Therefore, depending on the choice generated by the activation function, the selected nodes focus on the values of different branching decisions, including action and feature weights.

To understand how a specific state observation influences a particular action distribution, we can visualize the decision route from the root to the chosen leaf node in RTCs with the input state. For a given specific observation, we also provide the action probability distribution for each layer.

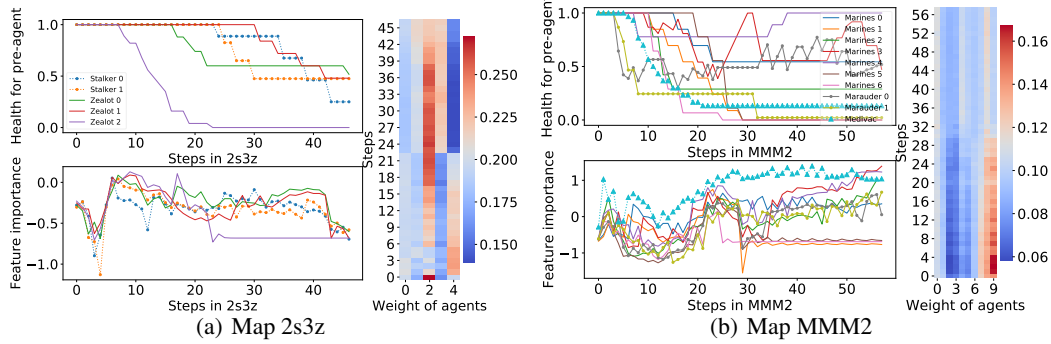


Figure 7: Importance of health attribute and weights of Q -values. As the number of steps increases, the degree of health importance in the line graph varies with the health of relevant agents. And in heatmaps, horizontal and vertical ordination indicate the agent-id and steps, respectively.

As shown in Fig. 6(b), we can receive the action probability distribution from each layer. Each node outputs a probability distribution with feature vectors, and the selected action depends on the probability linearly combined with the action distribution of each leaf node. From Fig. 6(b), we can find which features obtained more attention at each layer and how the features affect the action probability distribution. A detailed description is deferred to Appendix D.

Feature Importance. There are several ways of implementing feature importance assignment on soft decision trees [13], more details can be found in Appendix E. Considering that the data point is much easier to be perturbed into a false category or less confident of remaining in the original when there are multiple boundaries for partitioning the space, we utilize the decision confidence as a weight for assigning feature importance, which can positively be correlated with the distance from the instance to the decision boundary to relieve the above effects. Therefore, similar to Eq. 5, we weight the confidence probability of reaching the deepest non-leaf level node j as $P^j(o_i^t, h_i^{t-1})$. Then, the feature importance can be expressed by multiplying the confidence value with each decision node as

$$I(o_i^t) = \sum_j P^j(o_i^t, h_i^{t-1}) w_o^j. \quad (13)$$

After obtaining learned RTCs, we evaluated the feature importance of agents on different maps with Eq. 13. Fig. 7 presents the importance of health attributes and the weight of each agent for one episode. For the 2s3z scenario, we can find that Stalkers and Zealots each have similar feature importance at different steps, which could be sourced from the fact that they all focus on their health and play an equally important role in the battle. Notably, the Zealot 0 obtains a higher magnitude of the weight with a more intense the color in the heatmap at the 17 step since it may be attacked, resulting in a decrease in health value. Besides, when the health value of the Zealot 2 is 0, we also find it achieves strongly negative weights with blue shades, where the agent does not play an active role in battle since it is killed. Similar interesting findings exist in MMM2, where Medivac with agent-id 9 owns higher weights than the other agents during the early learning stage because Medivac is vital in combat to communicate the health of each agent. By analyzing the feature importance for each agent, we receive meaningful implicit knowledge of the tasks, which can facilitate human understanding of why particular feature importance leads to a certain action distribution. More details based on different features and analysis of stability are provided in Appendix E.

6 Conclusion

This paper presented MIXRTs, a novel interpretable multi-agent RL architecture based on the soft decision tree with recurrent structure. MIXRTs allows end-to-end training in a centralized fashion and learns to linearly factorize a joint action-value function for executing decentralized policies. The empirical results show that MIXRTs achieves model interpretability and scalability while maintaining competitive performance. Our approach captures the implicit knowledge of the challenging tasks with a transparent model and facilitates understanding of the learned domain knowledge and how input states influence decisions, which paves the application process in high-stake domains. We will focus on more practical explainable MARL techniques in the near future.

References

- [1] Yongcan Cao, Wenwu Yu, Wei Ren, and Guanrong Chen. An overview of recent progress in the study of distributed multi-agent coordination. *IEEE Transactions on Industrial Informatics*, 9(1):427–438, 2012.
- [2] Oriol Vinyals, Igor Babuschkin, Wojciech M Czarnecki, Michaël Mathieu, Andrew Dudzik, Junyoung Chung, David H Choi, Richard Powell, Timo Ewalds, Petko Georgiev, et al. Grandmaster level in starcraft ii using multi-agent reinforcement learning. *Nature*, 575(7782):350–354, 2019.
- [3] Zachary C Lipton. The mythos of model interpretability. *Queue*, 16(3):31–57, 2018.
- [4] Erico Tjoa and Cuntai Guan. A survey on explainable artificial intelligence (XAI): Toward medical XAI. *IEEE Transactions on Neural Networks and Learning Systems*, 32(11):4793–4813, 2020.
- [5] Manisha Natarajan and Matthew Gombolay. Effects of anthropomorphism and accountability on trust in human robot interaction. In *Proceedings of ACM/IEEE International Conference on Human-Robot Interaction*, pages 33–42, 2020.
- [6] Abhinav Verma. Verifiable and interpretable reinforcement learning through program synthesis. In *Proceedings of the AAAI Conference on Artificial Intelligence*, pages 9902–9903, 2019.
- [7] Zhengyao Jiang and Shan Luo. Neural logic reinforcement learning. In *International Conference on Machine Learning*, pages 3110–3119. PMLR, 2019.
- [8] David Silver, Aja Huang, Chris J Maddison, Arthur Guez, Laurent Sifre, George Van Den Driessche, Julian Schrittwieser, Ioannis Antonoglou, Veda Panneershelvam, Marc Lanctot, et al. Mastering the game of go with deep neural networks and tree search. *Nature*, 529(7587):484–489, 2016.
- [9] Nicholas Frosst and Geoffrey Hinton. Distilling a neural network into a soft decision tree. *arXiv preprint arXiv:1711.09784*, 2017.
- [10] Andrew Silva, Matthew Gombolay, Taylor Killian, Ivan Jimenez, and Sung-Hyun Son. Optimization methods for interpretable differentiable decision trees applied to reinforcement learning. In *International Conference on Artificial Intelligence and Statistics*, pages 1855–1865. PMLR, 2020.
- [11] Alberto Suárez and James F Lutsko. Globally optimal fuzzy decision trees for classification and regression. *IEEE Transactions on Pattern Analysis and Machine Intelligence*, 21(12):1297–1311, 1999.
- [12] Youri Coppens, Kyriakos Efthymiadis, Tom Lenaerts, Ann Nowé, Tim Miller, Rosina Weber, and Daniele Magazzeni. Distilling deep reinforcement learning policies in soft decision trees. In *Proceedings of the IJCAI 2019 Workshop on Explainable Artificial Intelligence*, pages 1–6, 2019.
- [13] Zihan Ding, Pablo Hernandez-Leal, Gavin Weiguang Ding, Changjian Li, and Ruitong Huang. Cdt: Cascading decision trees for explainable reinforcement learning. *arXiv preprint arXiv:2011.07553*, 2020.
- [14] Greg Brockman, Vicki Cheung, Ludwig Pettersson, Jonas Schneider, John Schulman, Jie Tang, and Wojciech Zaremba. Openai gym. *arXiv preprint arXiv:1606.01540*, 2016.
- [15] Mikayel Samvelyan, Tabish Rashid, Christian Schroeder De Witt, Gregory Farquhar, Nantas Nardelli, Tim GJ Rudner, Chia-Man Hung, Philip HS Torr, Jakob Foerster, and Shimon Whiteson. The starcraft multi-agent challenge. In *Proceedings of the International Joint Conference on Autonomous Agents and MultiAgent Systems*, AAMAS, 2019.
- [16] Tabish Rashid, Mikayel Samvelyan, Christian Schroeder, Gregory Farquhar, Jakob Foerster, and Shimon Whiteson. Qmix: Monotonic value function factorisation for deep multi-agent reinforcement learning. In *International Conference on Machine Learning*, pages 4295–4304. PMLR, 2018.

[17] Kyunghwan Son, Daewoo Kim, Wan Ju Kang, David Earl Hostallero, and Yung Yi. Qtran: Learning to factorize with transformation for cooperative multi-agent reinforcement learning. In *International Conference on Machine Learning*, pages 5887–5896. PMLR, 2019.

[18] Frans A Oliehoek and Christopher Amato. *A concise introduction to decentralized POMDPs*. Springer, 2016.

[19] Peter Sunehag, Guy Lever, Audrunas Gruslys, Wojciech Marian Czarnecki, Vinicius Zambaldi, Max Jaderberg, Marc Lanctot, Nicolas Sonnerat, Joel Z Leibo, Karl Tuyls, et al. Value-decomposition networks for cooperative multi-agent learning based on team reward. In *Proceedings of International Conference on Autonomous Agents and MultiAgent Systems*, pages 2085–2087, 2018.

[20] Ling Pan, Tabish Rashid, Bei Peng, Longbo Huang, and Shimon Whiteson. Regularized softmax deep multi-agent Q-learning. *Advances in Neural Information Processing Systems*, 34, 2021.

[21] Christopher JCH Watkins and Peter Dayan. Q-learning. *Machine Learning*, 8(3):279–292, 1992.

[22] Volodymyr Mnih, Koray Kavukcuoglu, David Silver, Andrei A Rusu, Joel Veness, Marc G Bellemare, Alex Graves, Martin Riedmiller, Andreas K Fidjeland, Georg Ostrovski, et al. Human-level control through deep reinforcement learning. *Nature*, 518(7540):529–533, 2015.

[23] Frans A Oliehoek, Matthijs TJ Spaan, and Nikos Vlassis. Optimal and approximate q-value functions for decentralized pomdps. *Journal of Artificial Intelligence Research*, 32:289–353, 2008.

[24] Landon Kraemer and Bikramjit Banerjee. Multi-agent reinforcement learning as a rehearsal for decentralized planning. *Neurocomputing*, 190:82–94, 2016.

[25] Ozan Irsoy, Olcay Taner Yildiz, and Ethem Alpaydin. Soft decision trees. In *Proceedings of International Conference on Pattern Recognition*, pages 1819–1822. IEEE, 2012.

[26] Dmitry Laptev and Joachim M Buhmann. Convolutional decision trees for feature learning and segmentation. In *German Conference on Pattern Recognition*, pages 95–106. Springer, 2014.

[27] Matthew Hausknecht and Peter Stone. Deep recurrent Q-learning for partially observable mdps. In *AAAI Fall Symposium on Sequential Decision Making for Intelligent Agents*, 2015.

[28] Cha Zhang and Yunqian Ma. *Ensemble machine learning: Methods and applications*. Springer, 2012.

[29] Hussein Hazimeh, Natalia Ponomareva, Petros Mol, Zhenyu Tan, and Rahul Mazumder. The tree ensemble layer: Differentiability meets conditional computation. In *International Conference on Machine Learning*, pages 4138–4148. PMLR, 2020.

[30] Philip Derbeko, Ran El-Yaniv, and Ron Meir. Variance optimized bagging. In *European Conference on Machine Learning*, pages 60–72. Springer, 2002.

[31] Ming Tan. Multi-agent reinforcement learning: Independent vs. cooperative agents. In *Proceedings of International Conference on Machine Learning*, pages 330–337, 1993.

[32] Ardi Tampuu, Tambet Matiisen, Dorian Kodelja, Ilya Kuzovkin, Kristjan Korjus, Juhan Aru, Jaan Aru, and Raul Vicente. Multiagent cooperation and competition with deep reinforcement learning. *PloS one*, 2017.

[33] Jian Hu, Siyang Jiang, Seth Austin Harding, Haibin Wu, and SW Liao. Rethinking the implementation tricks and monotonicity constraint in cooperative multi-agent reinforcement learning. *arXiv preprint arXiv:2102.03479*, 2021.

A Proof

Theorem 1. A factorizable joint action-value function $Q_{tot}(\tau, \mathbf{u})$ is factorized by individual action-value functions $Q_i(\tau_i, u_i)$ with weight $W_i = \frac{\exp(\phi_i)}{\sum_{i=1}^n \exp(\phi_i)}$, $\forall i \in \{1, 2, \dots, n\}$, ϕ_i representing a static distribution for mixing trees, such that the following holds

$$\arg \max_{\mathbf{u}} Q_{tot}(\tau, \mathbf{u}) = \left(\arg \max_{u_1} Q_1(\tau_1, u_1), \dots, \arg \max_{u_n} Q_n(\tau_n, u_n) \right),$$

then, we can say that individual action-value functions Q_i satisfy the IGM principle for joint action-value function Q_{tot} .

Proof. For an arbitrary factorizable $Q_{tot}(\tau, \mathbf{u})$, we take $\mathbf{u}^* = \arg \max_{\mathbf{u}} Q_{tot}(\tau, \mathbf{u})$. Recall that $\mathbf{u}^* := [u_i^*]_{i=1}^n \in \mathcal{U}^n$ and $u_i^* = \arg \max_{u_i} Q_i(\tau_i, u_i)$. Since the weights of each individual action-value function satisfy $W_i \in (0, 1)$, $\forall i \in \{1, 2, \dots, n\}$, for any given value function Q_i that satisfies Eq. 8, we have that

$$\frac{\partial Q_{tot}}{\partial Q_i} > 0. \quad (14)$$

Then, the following holds for any $[u_i]_{i=1}^n$ and the mixing trees function $Q_{tot}(\cdot)$ with n weights

$$\begin{aligned} & Q_{tot}(Q_1(\tau_1, u_1), Q_2(\tau_2, u_2), \dots, Q_n(\tau_n, u_n)) \\ &:= W_1 Q_1(\tau_1, u_1) + W_2 Q_2(\tau_2, u_2) + \dots + W_n Q_n(\tau_n, u_n) \\ &\leq W_1 Q_1(\tau_1, u_1^*) + W_2 Q_2(\tau_2, u_2^*) + \dots + W_n Q_n(\tau_n, u_n) \\ &\leq W_1 Q_1(\tau_1, u_1^*) + W_2 Q_2(\tau_2, u_2^*) + \dots + W_n Q_n(\tau_n, u_n) \\ &\dots \\ &\leq W_1 Q_1(\tau_1, u_1^*) + W_2 Q_2(\tau_2, u_2^*) + \dots + W_n Q_n(\tau_n, u_n^*). \end{aligned}$$

Thus, similar to the QMIX [16], the maximiser of the joint action-value is

$$\begin{aligned} & \max_{\mathbf{u}=(u_1, \dots, u_n)} Q_{tot}(\tau, \mathbf{u}) \\ &:= \max_{\mathbf{u}} Q_{tot}(Q_1(\tau_1, u_1), Q_2(\tau_2, u_2), \dots, Q_n(\tau_n, u_n)) \\ &= Q_{tot}(Q_1(\tau_1, u_1^*), Q_2(\tau_2, u_2^*), \dots, Q_n(\tau_n, u_n^*)). \end{aligned}$$

Hence, we have $\mathbf{u}^* = \arg \max_{\mathbf{u}} Q_{tot}(\tau, \mathbf{u})$ that satisfies the IGM principle, and the assumed mixing trees provide universal function approximation weights by Eq. 8. \square

B Experimental Details

B.1 StarCraft II Description

All implementations of algorithms are based on StarCraft II unit micro-management tasks (SC2.4.10 version). We consider combat scenarios where the enemy units are controlled by a built-in AI with the *difficulty*=7 setting, and each allied unit is controlled by the decentralized agents with reinforcement learning. During battles, the agents seek to maximize the damage dealt to enemy units while minimizing damage received, and require a range of skills. We evaluate our method on a range of challenging combat scenarios, and Table 2 presents a brief introduction of these scenarios with symmetric/asymmetric agent types and varying agent numbers. To better interpret MIXRTs in such complicated tasks, here we present the concise description of the StarCraft Multi-Agent Challenge (SMAC) [15] again, including the observations, states, actions and rewards settings.

Observations and States. At each time step, each agent receives local observations within their field of view, including the following attributes for both allied and enemy units: distance, relative X, relative Y, health, shield, and unit type. All Protos units have shields, which act as a source of defense against attack and have the ability to regenerate if no further damage is dealt. Particularly, the Medivacs as healer units to communicate the health status of each agent during the battle. The unit type is maintained for distinguishing different kinds of units on heterogeneous scenarios (e.g. 2s3z

Table 2: The StarCraft multi-Agent challenge benchmark.

Scenarios Type	Map	Ally Units	Enemy Units	Total Steps
Easy	3m	3 Marines	3 Marines	1050K
	8m	8 Marines	8 Marines	1500K
	2s3z	2 Stalkers, 3 Zealots	2 Stalkers, 3 Zealots	1500K
	2s_vs_1sc	2 Stalkers	1 Spine Crawler	1500K
Hard	5m_vs_6m	5 Marines	6 Marines	2M
	3s5z	3 Stalkers, 5 Zealots	3 Stalkers, 5 Zealots	2M
	8m_vs_9m	8 Marines	9 Marines	2M
Super Hard	6h_vs_8z	6 Hydralisks	8 Zealots	2M
	MMM2	1 Medivac, 2 Marauders, and 7 Marines	1 Medivac, 3 Marauders, and 8 Marines	2M

and MMM2 in the experiment). Note that the agents can only observe the others if they are alive and within their line of sight range, which is set to 9. If a unit (for both allies and enemies) feature vector resets to all zeros, indicating its death or invisibility from another agent’s sight range. The global state is only available to agents during centralized training, which contains information of all units on the map. Finally, all features, including the global state and the observation of the agent, are normalized by their maximum values.

Action Space. Each unit takes an action from the discrete action set: no-op, stop, move [direction], and attack [enemy id]. Agents are allowed to move with a fixed movement amount in four directions: north, south, east, and west, where the unit is allowed to take the attack [enemy id] action only when the enemy is within its shooting range. Note that a dead unit can only take the no-op action, while a living unit cannot. Lastly, the maximum number of operations a living agent can perform is typically between 7 and 70, which depends on the different scenarios.

Rewards. The target goal is to maximize the win rate for each battle scenario. At each time step, the agents receive a shaped reward based on the hit-point damage dealt and enemy units killed, as well as a special bonus for winning the battle. Additionally, agents obtain a 10 positive bonus after killing each enemy and a 200 bonus when killing all enemies, which is consistent with the default reward function of the SMAC.

B.2 Hyperparameters Settings

We compare our method to widely investigated value decomposition baselines, including VDN [19], QMIX [16], and QTRAN [17], based on an open-source implementation of these algorithms¹. Besides, we compare with existing interpretable models of SDTs [9] and CDTs [13] that decompose the problem into a set of simultaneous single-agent problems via the independent Q -learning (IQL) [31, 32] structure, called as I-SDTs and I-CDTs, respectively. Similarly, for fair comparisons, we also implement RTCs with the IQL to verify the reliability of the module, called as I-RTCs. The hyperparameters and environmental settings of these algorithms are consistent with their source codes, referring to the SMAC configuration [15]. More details can be found in Table 3.

Table 3: Hyperparameters settings of value-based algorithms.

Method	Hyperparameter/Description	Value
Common Setting	Difficulty of the game	7
	Evaluate Cycle	5000
	Target Update Cycle	200
	Number of the epoch to evaluate agents	32
	Optimizer	RMSprop
	Discount Factor γ	0.99
	Batch Size	32
	Buffer Size	5000
	Anneal Steps for ε	50000
	Learning Rates	0.0005
VDN/QMIX	Agent RNN Dimension	64
	Mixing Network Dimension	32
QTRAN	Agent RNN Dimension	64
	Mixing Network Dimension	64
	Lambda-opt	1.0
	Lambda-nopt	1.0
I-SDTs	Agent Trees Depth	3
I-CDTs	Intermediate Variables Dimension	32
	Intermediate Feature Depth	3
	Decision Depth	3
I-RTCs	Agent Trees Ensemble Dimension	32
	Agent Trees Depth	3
MIXRTs	Agent Trees Ensemble Dimension	32
	Agent Trees Depth	3
	Mixing Trees Ensemble Dimension	16
	Mixing Trees Depth	3

During training time, all agents are credited with defeating all enemy units within a specified time limit after an episode, and the target network is updated once after training every 200 episodes. We pause the training process for every 5000 training timesteps, and test the win rate of each algorithm for 32 episodes with the greedy action selection in the decentralized execution manner. All the results are averaged over 8 runs with different seeds and are displayed in the style of $mean \pm std$. Our model runs from 1 hour to 15 hours per task with an NVIDIA RTX 3080TI GPU and an Intel i9-12900k CPU, depending on the complexity and the episode length limit of each scenario.

¹<https://github.com/starry-sky6688/MARL-Algorithms>

C Experiments on StarCraft II

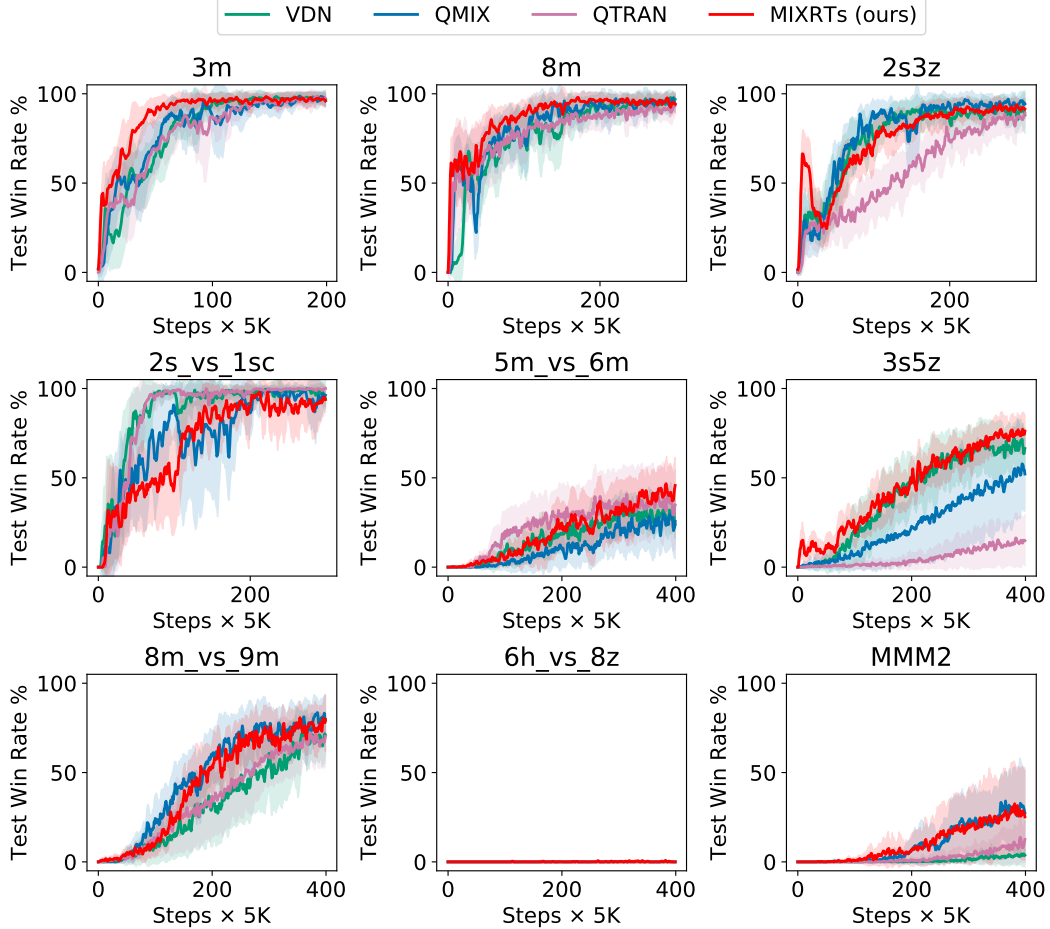


Figure 8: Median test win rates % on the different scenarios.

D Tree Structures in MARL

We show the structure of the trained MIXRTs model on map 3m with the individual action-value trees of the depth 3. By examining the learned filter at each observation with different weights, we can understand which essential features the RTCs considers assigning a particular action distribution to a particular state. Further, we display the action probability distribution at each layer of nodes for pre-agent (whose ids are 0, 1, and 2, respectively) based on the weights of the corresponding filters. It will get a more intense color in the heatmap when a particular observation feature obtains more attention with the higher magnitude of the weight. The color bars displayed on the left are the weight values of the features and output leaves, where shades of red relate to positive weights while blue shades represent negative weights.

Fig. 9 shows the learned filters from the root to the leaf of individual action-value RTCs of depth 3, where lines and arrows indicate the inference path. At the third level, the second node w_o^5 puts positive weights on the relative Y, relative X, and the health of the enemies 0 and 2 in the middle area. It is important to focus on the health, the relative X and Y of the goal attacked enemy to ensure that the enemy is within its shooting range, and make efficient damage dealt on the enemy units for each selected action. The left child leaf focuses on attacking the enemy 1 action, which may find the enemy 1 has low health within its shooting range, and taking the attack action can bring more bonus via more the priority than other actions. The right child leaf on its turns has strongly negative weights on attacking the enemy 0 and enemy 2. A possible reason for generating this particular choice is the

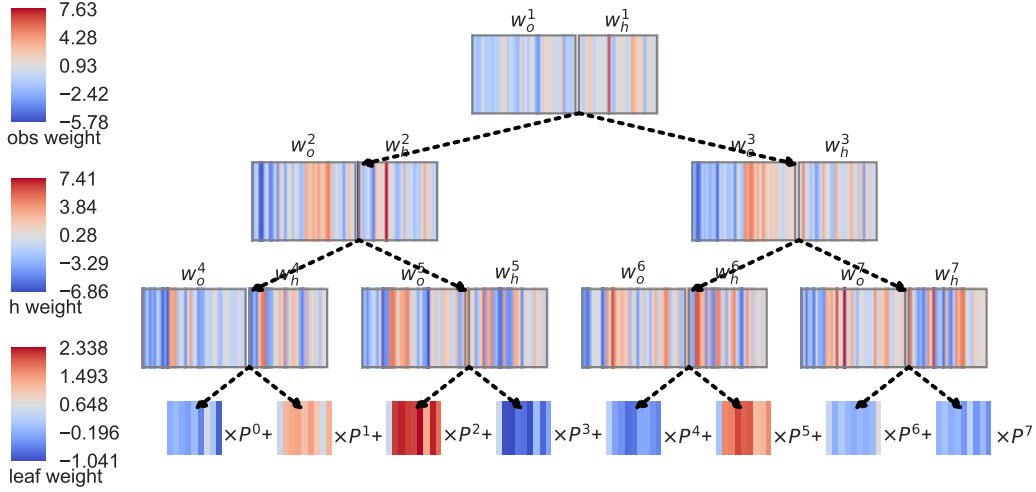


Figure 9: Heatmap visualization of the learned filters from the pre-agent of the RTCs.

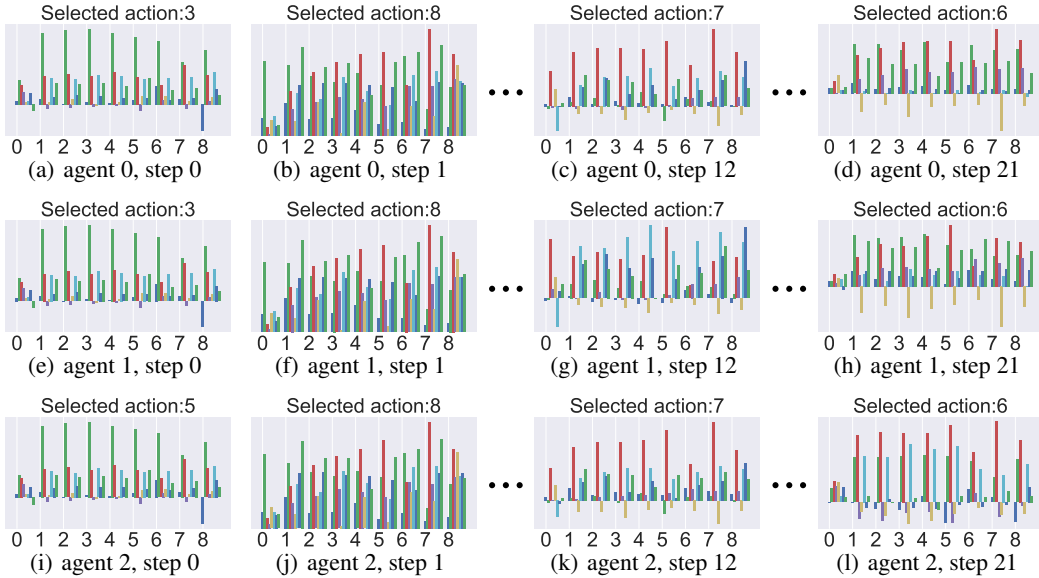


Figure 10: The action distributions learned by the leaf nodes of MIXRTs with depth 3 for three agents.

fact that the enemy 1 is out of the shooting range or in high health, where shooting the enemy 0 or enemy 2 can receive a more positive bonus. Depending on the case, the MIXRTs model gives us a concise decision process why the agent opts for some specific actions, which leads to an increased understanding of the explicit decision path with filters.

As shown in Fig. 10, we also demonstrate the output 8 leaf nodes of RTCs of depth 3 with all the action distributions for an episode on the 3m map. Three Marine agents execute 22 steps to achieve victory, as shown in subgraphs (a)-(d), (e)-(h) and (i)-(l), respectively. The digits on top of each leaf represent the selected action at this timestamp. Given a specific observation, we can obtain all the action distributions that RTCs provides in its leaves. We note that the agents tend to take the movement actions to find proper positions during the early stages of the phase, such as taking direction moving actions 2-5. Then most leaf distributions assign probabilities to actions related to attacking enemies (actions 6-8), and, interestingly, they are almost set to attack the same enemy at a particular timestamp. We can hereby determine that the MIXRTs has captured a policy of firepower for attacking the enemy whenever possible. Further, for each agent, the action 0 of each leaf node

always stays at a low selected probability when it is not killed in battle. From this, we can tell why the agent will indeed not consider taking action 0. One main reason is that the alive agents can receive more positive bonuses instead of taking action 0 to check whether they are alive or not, where the obtained high-level tactical behavior can be sourced from understanding the task. Inspecting the present action distributions in the leaves allows us to gain insights into the adopted strategies of the agent, which directly leads to increased interpretability of the learned behavior of the policy.

E Feature Importance and Agents Weighting Analysis

E.1 Feature Importance Assignment

To better analyze the learned MIXRTs model, we employ the assigned feature importance within each node as the metric. Throughout a local explanation, we can directly derive the inference process and the decision path of the learned MIXRTs. For global explanation, the feature importance of each agent over an episode can be averaged to obtain the global feature importance. There are several ways of implementing feature importance assignment on soft decision trees [13]. Several methods of feature importance assessment for input importance vector I with the same dimension as the decision node vectors w are listed as follows.

- An intuitive method for feature importance assignment on MIXRTs is simply adding the weight vectors of all nodes along the decision path $I(\mathbf{x}) = \sum_{k,j} w_k^j(\mathbf{x})$, k is the k -th layer.
- The second method to assign feature importance to MIXRTs is that we apply gradient-based methods to it: $I(\mathbf{x}) = \frac{\partial y}{\partial \mathbf{x}}$, where $y = \text{RTCs}(\mathbf{x})$.
- The third method is to sum all the weight vectors of nodes on the decision path: $I(o_i^t) = \sum_j w_o^j$, where j is the selected node on the probability route. However, due to the nature of shared parameters [19], this local explanation is indistinguishable for each agent. Therefore, we use Eq. 13 to describe the local explanation among different agents. Considering that the data point is much easier to be perturbed into a false category or less confident of remaining in the original when there are multiple boundaries for partitioning the space, we utilize the decision confidence as a weight for assigning feature importance. Above operation can positively be correlated with the distance from the instance to the decision boundary to relieve the above effects. Therefore, similar to Eq. 5, we weight the confidence probability of reaching the deepest non-leaf level node j as $P^j(o_i^t, h_i^{t-1})$. Then, the feature importance can be expressed by multiplying the confidence value with each decision node as $I(o_i^t) = \sum_j P^j(o_i^t, h_i^{t-1})w_o^j$.

E.2 Results of Feature Importance

As shown in Fig. 11, we select three properties of the agent to indicate their importance and display the weight of individual Q -values across an episode, including own health, enemy distance and relative Y properties. We analyze the three properties on three different maps, and the results are shown in Figs. 11(a), 11(c) and 11(e), respectively. The horizontal coordinate and the vertical coordinate represent the number of steps in the episode and the size of the corresponding value, respectively. Meanwhile, we visualize the weights W_i for each agent i on each step during each scenario, and the weight heatmaps are shown in Figs. 11(b), 11(d) and 11(f). In the attention heatmaps, the steps increase from bottom to top, and the horizontal ordination indicates the agent id.

For 8m, it is essential to achieve a victory that the agents avoid being killed and pay more attention to firepower for killing the enemies. From Fig. 11(a), we observe that allies have similar feature importance on the same attribute. It is worth noting that when an enemy is killed in combat, both the value of the importance of the distance of this enemy and relative Y will decrease. It suggests that RTCs can understand the tasks and generate coping actions when the environment changes. In addition, as shown in Fig. 11(b), we can find that each agent has almost equal attention weights, which means that each allied Marines plays a similar role on the homogeneous scenario and MIXRTs almost equally divides Q_{tol} for each agent. MIXRTs performs well with the refined mixing trees since it adjusts weights of Q_i with a minor difference.

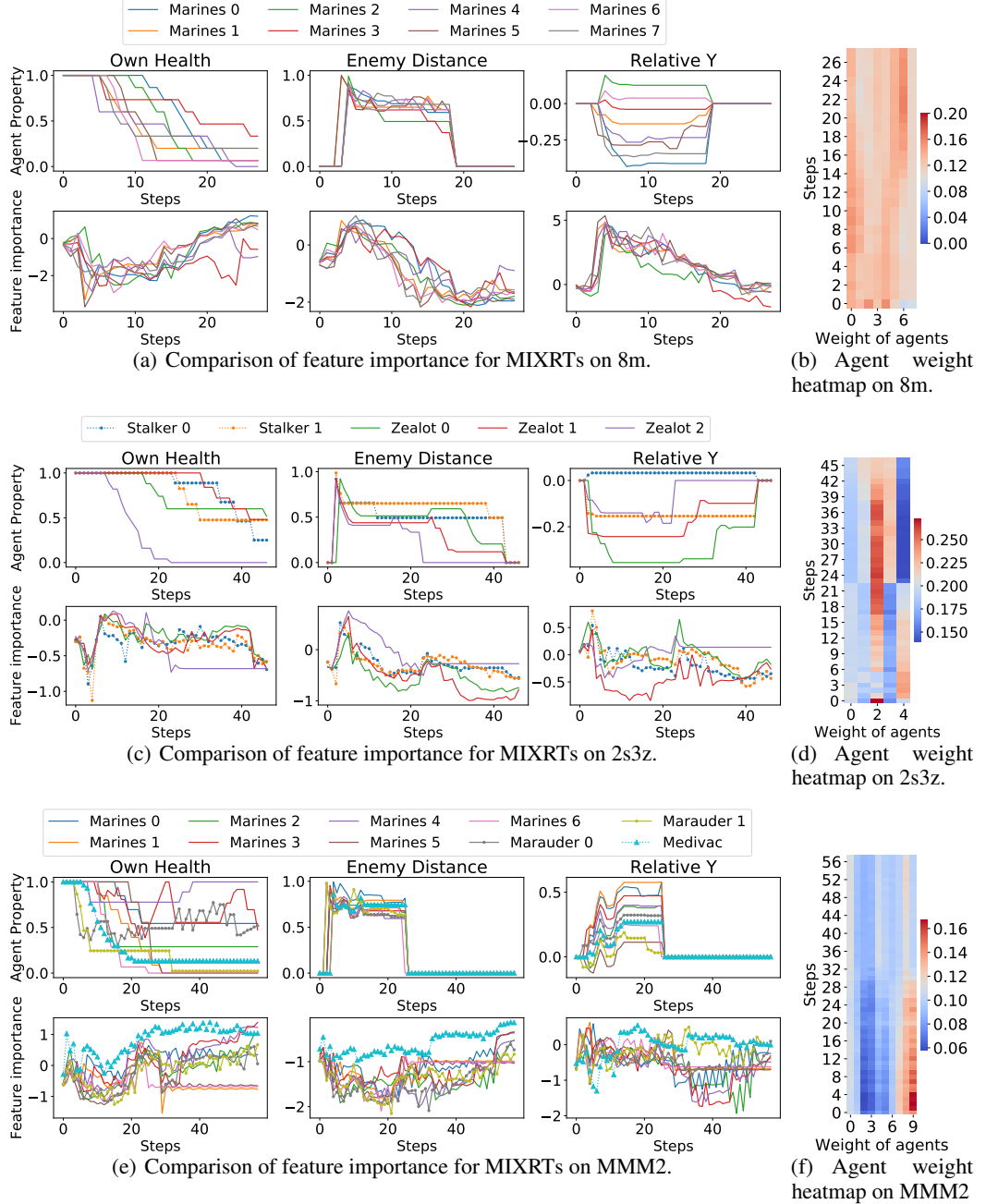
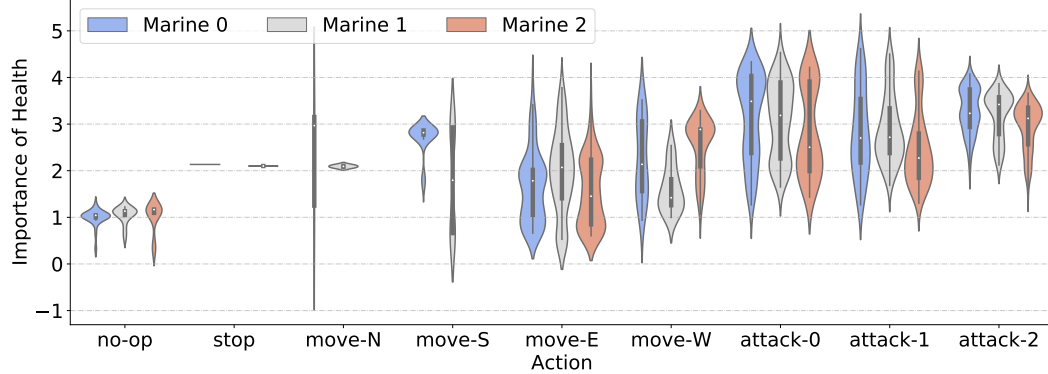
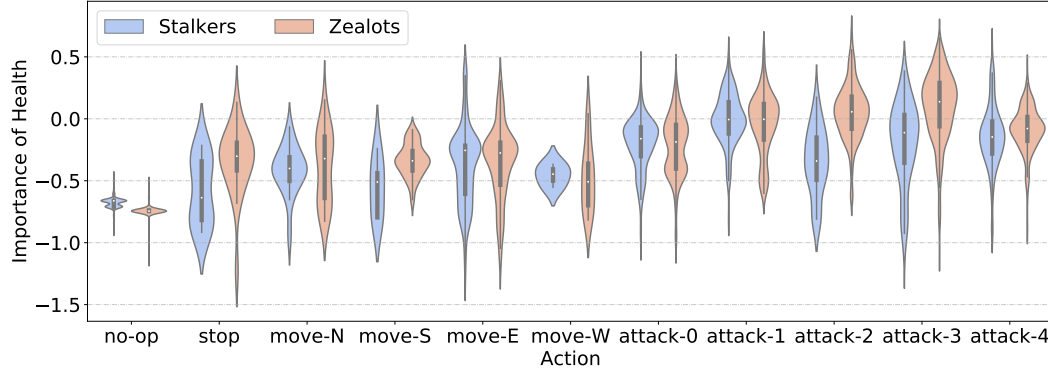


Figure 11: Feature importance and the assigned weights of Q -values of the agent.

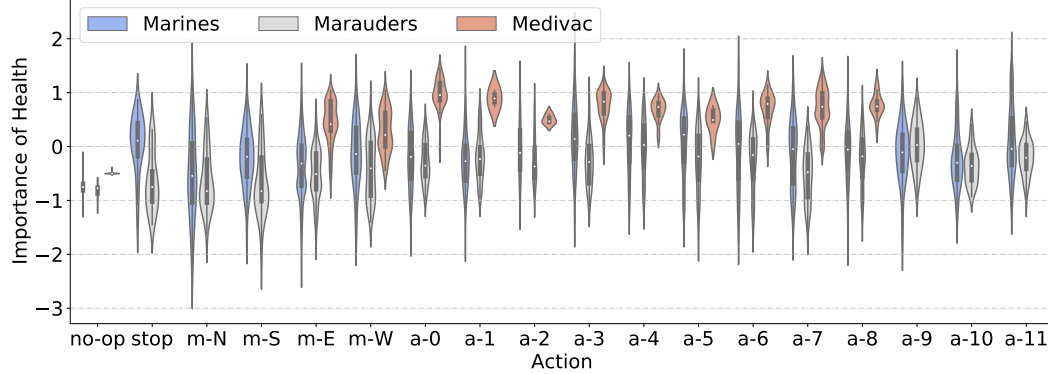
The more pronounced weight differences on the heterogeneous scenarios 2s3z and MMM2 are also illustrated in Figs. 11(c)-11(f). After analyzing the feature importance and the correlation between agent features, it is of interest that the drastic change in the weight of the agents on 2s3z since the replacement of Zealot 2 by Zealot 0 after its death in battle, as shown in Fig. 11(d). Meanwhile, Zealot 0 will be moving closer to the enemy at the 24-th step, and the distance and health importance will increase. Furthermore, as shown in Fig. 11(f), we notice that different types of soldiers have different sensitivity to features. For example, Medivac (agent 9) receives more attention during the early stages of the battle, which may be attributed to their different roles involved in combat. In summary, the MIXRTs approximation method is capable of capturing the impact of the sophisticated observations in a battle and better explaining the sub-spaces for Q_{tot} decomposition.



(a) Violin plot showing the feature importance on 3m.



(b) Violin plot showing the feature importance on 2s3z.



(c) Violin plot showing the feature importance on MMM2.

Figure 12: Violin plots showing the feature importance of fitted MIXRTs on 32 episodes.

E.3 Analysis of Stability on Feature Importance.

The stability of the interpretable model is an important factor reflecting the reliability. To further study the stability, we take a deeper look into MIXRTs itself in terms of the assigned feature importance and the action distributions. We conduct analyses with the violin plot to study the distribution of action among several episodes. With the violin plot, it would be beneficial for us to immediately identify the median feature importance size without having to visually estimate it by integrating the density, which can help us receive strictly more information and analyze the stability of feature importance. Wider sections of the violin plot represent a more dense distribution, the thinner sections correspond to a more sparse distribution. We hope this can alleviate the differences in action distributions caused by the different initialized states at the beginning of each episode.

As shown in Fig. 12, we select the health property of the agents to indicate the correlation between the underlying action distribution and the assigned feature importance over 32 episodes. We analyze the health property on the three different maps, and the results are shown in Figs. 12(a), 12(b) and 12(c). The horizontal coordinate and the vertical coordinate represent the selected action and the importance of the health of the agent itself, respectively.

For 3m scenario, it requires the three allied agents to pay more attention to firepower to kill the enemies with fewer casualties. As shown in Figs. 12(a), we can observe that the three allies own similar importance among all the actions, which aligns with the common knowledge that homogeneous agents play the same important role during the battles. Besides, we also find that they pay more attention to selecting attack actions, which may mean that it can bring more positive rewards to ensure victory than taking the other actions in this easy homogeneous agent environment. The findings are similar to the idea of 8m, meaning that MIXRTs have mastered the tasks and generate coping actions when the environment changes over several episodes.

From Figs. 12(b) and 12(c), considerable differences can also be spotted over 32 episodes on the heterogeneous scenarios 2s3z and MMM2, even though MIXRTs have captured similar skills to win. For 2s3z scenario, we see Zealots obtain higher importance of health than Stalkers, which may require a better winning strategy where Zealots agents serve at the front of combat, killing enemies one after another while protecting the Stalkers to kite the enemy around the map. Furthermore, we notice that similar interesting findings also exist on MMM2 scenario. For example, Medivac, as a healer unit, receives more attention than other kinds of agents during the battle. This could lead the cooperative team to more effectively defeat the enemies since Medivac uses healing actions to improve the health of the teammates. We also still obtain meaningful and interesting implicit knowledge of the tasks that is also consistent with the above analysis in subsection 5.2.

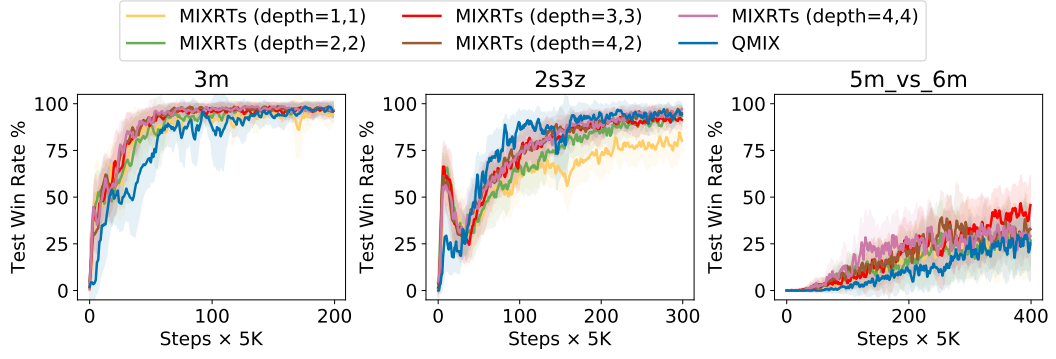
Overall, the importance of health is slightly higher when the agents are in attacking status than in moving status, and significantly higher when not operating. Since on most occasions when the agents are attacking, they are also being attacked, the importance of health is more intense. Meanwhile, being killed agents receive the negative importance of health with a small interquartile range, which is consistent with the case study above. As far as stability is concerned, the non-operation of agents also maintains a steady state in the model since most of them own a health value of 0. In summary, even though the different initialized environments change, we could still find the implicit knowledge from MIXRTs by analyzing the feature importance over several episodes. It could enhance the trustworthiness of interpretability in terms of feature importance.

F Ablation Experiment for Tree Models

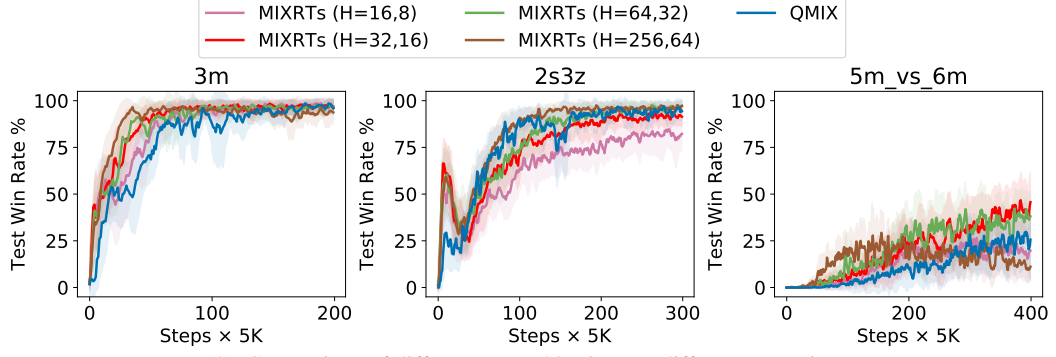
To analyze how sensitive MIXRTs is to the effect of tree depth of the action-value individual RTCs and the mixing trees, as well as the number of ensemble trees H on performance, we vary these factors for our experiments. Fig. 13(a) and Fig. 13(b) show respective effects of the above factors on the performance of MIXRTs.

First, we investigate the influence of different depths of the action-value on the individual RTCs and the mixing trees using three scenarios. Fig. 13(a) shows the ablation results that the performance of MIXRTs will improve when the depth of the individual RTCs and the mixing of RTCs appropriately increase. Generally, a moderate depth (e.g., depth=2, 2) setting can obtain a better performance, where the former 2 and the latter 2 represent the depth of the individual action-value RTCs and mixing RTCs of MIXRTs with depth=2, 2, respectively. Besides, we study the effect of the number of ensemble trees on performance. Fig. 13(b) indicates that the tree model shows a clear tendency to be unstable when the tree depth or ensemble dimension is small. With moderate values (e.g., $H = 32 \sim 64$), the tree usually converges quickly and obtains better performance. It shows that a moderate depth and number of ensemble tree settings can achieve promising performance while retaining the simplicity and interpretability of the model. For this reason, we chose default parameters that are trade-offs between the two and comparable to the baselines, and more details can be found in Table 1.

We further analyze the stability of the interpretability of different trees when the depth of the tree increases on different scenarios. As shown in Fig. 14, I-SDTs and I-CDTs improve performance on simple maps by increasing the depth of the tree, but they do not work well with a rough approximation on hard scenarios. In contrast, I-RTCs with deeper levels (brown curves) can better perform on



(a) Comparison of different depths on different scenarios.



(b) Comparison of different ensemble sizes on different scenarios.

Figure 13: The effect of MIXRTs on performance with respect to the depth and the number of ensemble trees.

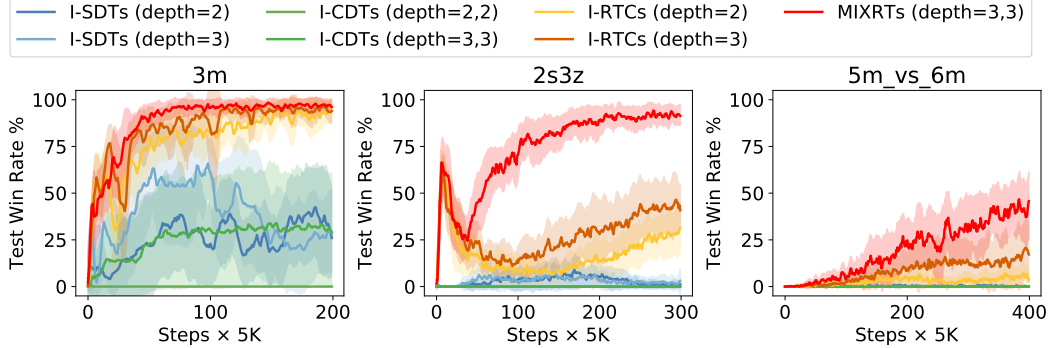


Figure 14: Comparison of I-SDTs, I-CDTs, I-RTCs and MIXRTs with different depths.

different scenarios since the ensemble trees structure and its capture of historical information. From the comparisons, MIXRTs is less sensitive to tree depth than other trees. It shows that MIXRTs effectively approximates the sophisticated relationship between Q_i and Q_{tot} with the mixing trees module to capture different features in sub-spaces.